for X-ray work. To date, only one crystal structure of a metal complex with bzp has been reported.[32] This compound contains the $[(Cu(bzp))_2C_2O_4]^{2+}$ cation, and bzp is bound to copper(II) through the nitrogen atoms of both the pyridine ring and the imine group. It has already been reported that bzp can induce a spin transition in iron(II) chemistry; indeed, $Fe(bzp)_2(NCS)_2$ presents such a transition around 235 K.[33] In **3**, the transition occurs at much the same temperature, but is more gradual and very incomplete since only 56% of the metal centers become low-spin upon cooling down. Another striking aspect of the phenomenon is that, below the transition temperature, the relative proportions of SS, QQ, and SQ species do not correspond at all to the statistical proportions. If 56% of the low-spin and 44% of the high-spin iron(II) were statistically distributed among the SS, QQ, and SQ species, we would have 31.4% of SS (instead of 52%), 19.4% of QQ (instead of 40%) and 49.3% of SQ (instead of 8%). In fact, when an iron(II) ion undergoes the transition within a dinuclear unit, the other iron(II) ion of the same unit has a very high probability of undergoing the transition too, so that the formation of SQ species is unlikely. In a certain sense, the dinuclear unit itself plays the role of a small domain in which the two metal ions have the same spin state.

To conclude, we may attempt to sum up the results emerging from this study: (i) The high-spin state in the dinuclear species seems to l e stabilized with respect to what happens with mononuclear species in which the iron(II) ion has much the same environment; (ii) the spin transition, when occurring, is apparently more gradual and very incomplete in the low-temperature range; (iii) the intramolecular interaction gives rise to a specific cooperativity within the dinuclear unit. In spite of the incomplete character of the transition, the proportion of electronically dissymmetric species SQ is very small.

It would be quite unreasonable to generalize the results presented above to all of the polymetallic systems in which spin transition and exchange interaction coexist. Many investigations will be necessary before an overview can be obtained on this problem.

Registry No. **1**, 109584-92-1; **2**, 109584-93-2; **3**, 109612-95-5; $Fe(py)_4(NCS)_2$, 15154-78-6.

Supplementary Material Available: Listings of atomic parameters for hydrogen atoms (Table S1) and anisotropic thermal parameters for non-hydrogen atoms (Table S2) (2 pages); a table of calculated and observed structure factors (9 pages). Ordering information is given on any current masthead page.

(32) Real, J. A.; Borras, J.; Solans, X.; Font-Altaba, M. *Transition Met. Chem. (Weinheim, Ger.)*, in press.
(33) Real, J. A.; Borras, J.; Adler, P.; Gütlich, P., unpublished result.

Contribution from the Departments of Chemistry, Northwestern University, Evanston, Illinois 60208, and Oklahoma State University, Stillwater, Oklahoma 74078

Synthesis of Heterometallic Carbide Clusters Containing Three Iron Atoms: $[PPN]_2[MFe_3(CO)_{13}C]$ (M = Cr, W), $[PPN]_2[Cr_2Fe_3(CO)_{16}C]$, $Rh_2Fe_3(CO)_{14}C$, and $[PPN][Rh_3Fe_3(CO)_{15}C]$

Joseph A. Hriljac,[†] Elizabeth M. Holt,*[‡] and Duward F. Shriver*[†]

Received January 14, 1987

Redox-condensation reactions involving $[PPN]_2[Fe_3(CO)_9(CCO)]$ and electrophilic transition-metal reagents lead to $[PPN]_2[MFe_3(CO)_{13}C]$ (M = Cr, W), $[PPN]_2[Cr_2Fe_3(CO)_{16}C]$, $Rh_2Fe_3(CO)_{14}C$, and $[PPN][Rh_3Fe_3(CO)_{15}C]$. Variable-temperature ^{13}C NMR spectroscopy was employed to assign the structures of the tetranuclear clusters and $Rh_2Fe_3(CO)_{14}C$ in solution. An improved synthesis of $[PPN][RhFe_3(CO)_{12}C]$ and more complete variable-temperature (ca. −130 to +20 °C) ^{13}C NMR spectra of this cluster and $[PPN][MnFe_3(CO)_{13}C]$ are discussed. All of the tetranuclear clusters are assigned butterfly metal geometries with the heterometals located at hinge sites. Attempts to prepare iron–molybdenum carbide clusters are discussed. The structure of $[PPN][Rh_3Fe_3(CO)_{15}C]$ was determined by a single-crystal X-ray diffraction study and was found to consist of a trigonal-antiprismatic metal array with the carbide ligand within the metal polyhedron. The iron atoms define one of the trigonal faces and the rhodium atoms define the other. Crystal data for $[PPN][Rh_3Fe_3(CO)_{15}C]$: monoclinic, space group $P2_1/n$, a = 16.220 (6) Å, b = 9.282 (3) Å, c = 35.17 (3) Å, β = 94.84 (5)°, Z = 4.

Introduction

Transition-metal carbide clusters form a very interesting class of organometallic compounds. These clusters contain a carbon atom bonded only to metal atoms, and therefore their study plays a central role in defining the structural, bonding, and reactivity aspects of metal–carbon bonds. They may also be useful as models of the reactive carbide species that form on metal surfaces during CO hydrogenation reactions.[1,2]

The first report of reactivity at a carbide ligand was by Bradley and co-workers,[3] who demonstrated that the carbide ligand in a butterfly cluster with four metal atoms is subject to attack. This is in contrast to what had been found earlier for pentametallic clusters.[4,5] Studies of these butterfly cluster compounds by several research groups have demonstrated that reactions of the carbide ligands can lead to the formation of C–H and C–C bonds.[2,6]

Carbide reactivity is unique to the tetranuclear butterfly clusters. It was therefore of interest to study similar systems to try to understand the factors that relate to this reactivity and to try and extend the known reaction pathways. This work is directed toward the synthesis of new heterometallic carbide clusters, especially those that should contain reactive carbide ligands. The synthetic methodology that was chosen was to use the trimetallic cluster $[Fe_3(CO)_9(CCO)]^{2-}$ in redox-condensation reactions.[7] We previously demonstrated that this ketenylidene cluster is a useful carbide precursor.[8,9]

[†] Northwestern University.
[‡] Oklahoma State University.

(1) Tachikawa, M.; Muetterties, E. L. *Prog. Inorg. Chem.* **1981**, *28*, 203 and references therein.
(2) Bradley, J. S. *Adv. Organomet. Chem.* **1983**, *22*, 1 and references therein.
(3) Bradley, J. S.; Ansell, G. B.; Hill, E. W. *J. Am. Chem. Soc.* **1979**, *101*, 7417.
(4) Cooke, C. G.; Mays, M. J. *J. Organomet. Chem.* **1975**, *88*, 231.
(5) Kolis, J. W.; Basolo, F.; Shriver, D. F. *J. Am. Chem. Soc.* **1982**, *104*, 5626.
(6) Bogdan, P. L.; Woodcock, C.; Shriver, D. F. *Organometallics*, **1987**, *6*, 1377.
(7) Chini, P.; Heaton, B. T. *Top. Curr. Chem.* **1977**, *71*, 1.
(8) Kolis, J. W.; Holt, E. M.; Hriljac, J. A.; Shriver, D. F. *Organometallics* **1984**, *3*, 496.
(9) Hriljac, J. A.; Swepston, P. N.; Shriver, D. F. *Organometallics* **1985**, *4*, 158.

0020-1669/87/1326-2943$01.50/0

This research led to the synthesis of tetra-, penta-, and hexametal cluster compounds. Details of the synthesis and characterization of several heterometallic carbide systems are discussed, and an improved synthesis of $[PPN][RhFe_3(CO)_{12}C]$[9] is described.

Experimental Section

General Procedures and Materials. All of the compounds prepared in this work are moderately air- and moisture-sensitive, and therefore all manipulations were performed under an atmosphere of purified nitrogen by employing standard Schlenk and needlestock techniques.[10,11] Solids were manipulated in a Vacuum Atmosphere glovebox equipped with a recirculator and Dri-Train system. Solvents were refluxed over and then distilled from appropriate drying agents under nitrogen before use (THF, Et_2O, and hexane from Na/benzophenone; acetone and pentane from 4A molecular sieves; dichloromethane from P_2O_5; methanol and 2-propanol from Mg/I_2; acetonitrile from CaH_2). NMR solvents were freeze/thaw-degassed and then vacuum-distilled from appropriate drying agents. The following starting materials were synthesized by literature methods (or minor variations thereof) and judged pure by IR spectroscopy: salts of $[Fe_3(CO)_9(CCO)]^{2-}$ and its ^{13}C-enriched analogues;[12] $[Rh(CO)_2Cl]_2$;[13] $Rh(CO)_2(py)Cl$;[14] $Cr(CO)_3(NCMe)_3$;[15] $W(CO)_3(NCEt)_3$.[16] GLASSCLAD6C was purchased from Petrarch Chemicals.

IR spectra were recorded with a Perkin-Elmer 283 spectrometer using 0.1 mm path length CaF_2 solution cells or Nujol mulls between KBr plates. ^{13}C NMR spectra were recorded with either a JEOL FX-270 or Varian XL-400 spectrometer operating at 67.8 and 100.577 MHz, respectively. All chemical shifts are reported positive if downfield from TMS, and the ^{13}C resonance for CD_2Cl_2 (53.80 ppm) was used as the reference peak. $Cr(acac)_3$ (acac = acetylacetonate) was added as a relaxation agent. Elemental analyses were performed by Galbraith Laboratories. Mass spectra were recorded by Dr. D. Hung of the Northwestern University Analytical Services Laboratory with a Hewlett-Packard HP5905A spectrometer using 70-eV ionization.

Synthesis of [PPN][$RhFe_3(CO)_{12}C$] (PPN = Bis(triphenylphosphine)nitrogen(1+)). All Schlenk flasks used in this preparation were treated with GLASSCLAD6C before use. A Schlenk flask was charged with 1.001 g (0.6514 mmol) of $[PPN]_2[Fe_3(CO)_9(CCO)]$, 0.178 g (0.651 mmol) of $Rh(CO)_2(py)Cl$ (py = pyridine), 0.193 g (0.654 mmol) of $[BzMe_3N][PF_6]$, and a magnetic stirbar. A 10-mL portion of dichloromethane was added and the solution stirred. After 20 min, 50 mL of Et_2O was added to the red-brown solution. The resulting precipitate was removed via filtration, the solution was cooled to 0 °C, and 50 mL of pentane was slowly introduced via syringe. The red microcrystalline solid was isolated and washed with pentane before drying under vacuum: 0.580 g isolated, 77% yield. Anal. Calcd (found) for $C_{49}H_{30}NFe_3RhO_{12}P_2$: C, 50.86 (50.34); H, 2.61 (2.62); N, 1.21 (1.17); Fe, 14.48 (13.37); Rh, 8.89 (9.38).

Synthesis of $[PPN)_2[CrFe_3(CO)_{13}C]$. A Schlenk flask was charged with 1.000 g (0.6507 mmol) of $[PPN]_2[Fe_3(CO)_9(CCO)]$, 0.190 g (0.733 mmol) of $Cr(CO)_3(NCMe)_3$, and a magnetic stirbar. The flask was immersed in a −23 °C (CCl_4 slush) cold bath, and 10 mL of acetone was slowly introduced via syringe. The solution was stirred 30 min and then 40 mL of 2-propanol added. Removing the cold bath and subsequent warming to room temperature produced a dark brown solid. The crude product was isolated by filtration and washed with three portions of methanol (5 mL each) and then thoroughly with Et_2O before vacuum drying. This material was recrystallized by the slow diffusion of Et_2O (30 mL) into a dichloromethane solution (15 mL) of the cluster: 0.990 g isolated, 91% yield. Anal. Calcd (found) for $C_{86}H_{60}N_2Fe_3CrO_{13}P_4$: C, 61.74 (61.34); H, 3.62 (3.96); N, 1.68 (1.88); Fe, 10.02 (9.88); Cr, 3.11 (2.22).

Synthesis of $[PPN]_2[WFe_3(CO)_{13}C]$. A Schlenk flask was charged with 1.000 g (0.6507 mmol) of $[PPN]_2[Fe_3(CO)_9(CCO)]$, 0.340 g (0.785 mmol) of $W(CO)_3(NCEt)_3$, and a magnetic stirbar. Addition of 10 mL of acetone followed by 20 min of stirring produced a dark greenish brown solution. The crude product was precipitated by the addition of 40 mL of 2-propanol. The solids were isolated and washed with three portions of methanol (5 mL each) and Et_2O before drying. Slow diffusion of Et_2O (35 mL) into a dichloromethane solution (20 mL) produced black crystals: 0.943 g isolated, 80% yield. Anal. Calcd (found) for $C_{86}H_{60}N_2Fe_3WO_{13}P_4$: C, 57.23 (56.38); H, 3.35 (3.11); N, 1.55 (1.74); Fe, 9.28 (9.01); W, 10.19 (10.28).

Table I. X-ray Crystal Structure Data for $[PPN][Rh_3Fe_3(CO)_{15}C]$

formula	$C_{52}H_{30}Fe_3NO_{15}P_2Rh_3$	V, Å^3	5276.2 (53)
mol wt	1446.97	d_{calcd}, g cm^{-3}	1.821
cryst habit	needle	$F(000)$	2848
cryst size, mm	<(0.3 × 0.3 × 0.5)	λ(Mo Kα), Å	0.71069
		μ(Mo Kα), cm^{-1}	18.32
cryst color	black	scan mode	θ–2θ
cryst syst	monoclinic	$2\theta_{max}$, deg	78
space group	$P2_1/n$	octants measd	$+h,+k,\pm l$
Z	4	total data	11064
a, Å	16.220 (6)	data, $I > 3\sigma(I)$	4476
b, Å	9.282 (3)	R,[a] %	6.3
c, Å	35.17 (3)		
β, deg	94.84 (5)		

[a] Function minimized $\sum w(|F_o| - |F_c|)^2$; $R = (\sum||F_o| - |F_c||)/\sum|F_o|$.

Synthesis of $[PPN)_2[Cr_2Fe_3(CO)_{16}C]$. A 0.500-g (0.325-mmol) sample of $[PPN]_2[Fe_3(CO)_9(CCO)]$ and 0.210 g (0.810 mmol) of $Cr(CO)_3(NCMe)_3$ were stirred in 5 mL of acetone for 2 h. The addition of 40 mL of methanol led to the precipitation of a dark brown solid. This material was isolated by filtration and washed with methanol and Et_2O before drying in vacuo. Recrystallization was accomplished by allowing Et_2O (20 mL) to slowly diffuse into a dichloromethane (10 mL) solution of the compound. The resulting black crystals were isolated and washed with methanol (5 mL) and Et_2O before the final drying: 0.402 g isolated, 68% yield. Anal. Calcd (found) for $C_{89}H_{60}N_2Fe_3Cr_2O_{16}P_4$: C, 59.09 (58.51); H, 3.34 (3.63); N, 1.55 (1.84); Fe, 9.26 (9.48); Cr, 5.75 (5.71).

Synthesis of $Rh_2Fe_3(CO)_{14}C$. All flasks in this preparation were treated with GLASSCLAD6C before use. A Schlenk flask was loaded with 0.500 g (0.432 mmol) of $[PPN][RhFe_3(CO)_{12}C]$, 0.160 g (0.412 mmol) of $[Rh(CO)_2Cl]_2$, and a magnetic stirbar. A 10-mL portion of Et_2O was added, and after 5 min of stirring, the solution was evaporated to dryness. The oily residue was extracted with 60 mL of warm (ca. 50 °C) hexane. The dark green solution was quickly filtered through a medium-porosity frit and concentrated to ca. 10 mL. After the solution was cooled to 0 °C for 1 h, the resulting black crystals were removed via filtration and dried: 0.184 g isolated, 57% yield. Anal. Calcd (found) for $C_{15}Fe_3Rh_2O_{14}$: C, 23.17 (22.99); Fe, 21.55 (21.66); Rh, 26.47 (26.89). Mass spectrum: parent ion at m/e 778 with stepwise loss of 14 CO's.

Synthesis of [PPN][$Rh_3Fe_3(CO)_{15}C$]. All flasks used in this preparation were treated with GLASSCLAD6C before use. A Schlenk flask was charged with 0.500 g (0.325 mmol) of $[PPN]_2[Fe_3(CO)_9(CCO)]$, 0.260 g (0.669 mmol) of $[Rh(CO)_2Cl]_2$, and a magnetic stirbar. A 10-mL portion of THF was added and the slurry stirred. After 2 h the dark red-brown solution was evaporated to dryness. The oily solids were extracted with 15 mL of a 1:1 mixture of Et_2O and 2-propanol. This extract was filtered through a medium-porosity frit, and 40 mL of pentane was slowly added with vigorous shaking. The resulting tacky dark red microcrystals were isolated, washed with pentane, and dried. Repeated recrystallizations from Et_2O/pentane produced black crystals in variable yields, typically 20–45%. Anal. Calcd (found) for $C_{52}H_{30}NFe_3Rh_3O_{15}P_2$: C, 43.16 (42.39); H, 2.09 (2.03); N, 0.97 (1.03); Fe, 11.58 (10.52); Rh, 21.34 (21.60).

X-ray Crystal Structure of [PPN][$Rh_3Fe_3(CO)_{15}C$]. Crystals suitable for analysis were obtained by diffusion of pentane into a Et_2O solution. These were sealed in thin-walled glass capillaries, and the crystal chosen for study was mounted on a Syntex P3 automated diffractometer. Unit-cell dimensions (Table I) were determined by the least-squares refinement of the best angular positions for 15 independent reflections ($2\theta > 15°$) during normal alignment procedures using molybdenum radiation. Data were collected at room temperature by using the parameters listed in Table I with a scan width of 0.8° below $K\alpha_1$ and 0.8° above $K\alpha_2$. The scan rate varied from 15 to 24.3° min^{-1} on the basis of the intensity recorded in a 10-s prescan. Backgrounds were measured at each side of the scan for a combined time equal to the total scan time. The intensities of 3 standard reflections were remeasured after every 97 reflections. These showed less than 8% variation, and no correction for decomposition was performed. Data were corrected for Lorentz, polarization, and background effects.

Heavy-atom positions were established by direct methods using MULTAN80.[17] Successive least-squares/difference Fourier cycles allowed

(10) Shriver, D. F.; Drezdzon, M. A. *The Manipulation of Air-Sensitive Compounds*, 2nd ed.; Wiley: New York, 1986.
(11) Brown, H. C. *Organic Synthesis via Boranes*; Wiley: New York, 1975.
(12) Hriljac, J. A.; Shriver, D. F. *J. Am. Chem. Soc.*, in press.
(13) McCleverty, J. A.; Wilkinson, G. *Inorg. Synth.* **1966**, *8*, 211.
(14) Lawson, D. N.; Wilkinson, G. *J. Chem. Soc.* **1965**, 1900.
(15) Tate, D. P.; Knipple, W. R.; Augl, J. M. *Inorg. Chem.* **1962**, *1*, 433.
(16) Kubas, G. J. *Inorg. Chem.* **1983**, *22*, 692.
(17) Main, P.; Fiske, S. J.; Hull, S. E.; Lessinger, L.; Germain, G.; Declercq, J.-P.; Woolfson, M. M. "MULTAN80"; University of York: York, England, 1980.

Scheme I

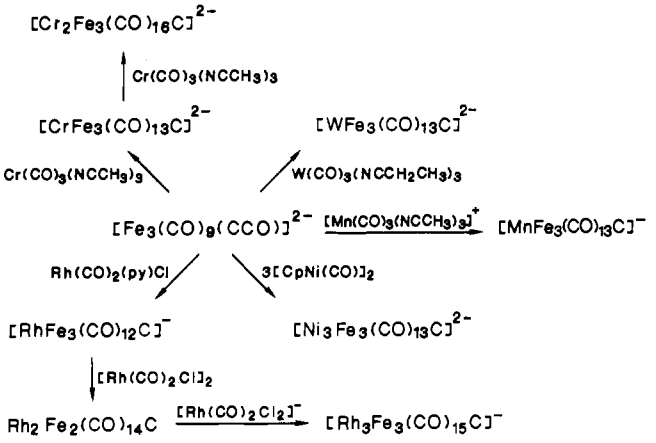

the location of the remainder of the non-hydrogen atoms. Refinement[18] of scale factor, positional, and anisotropic thermal parameters for all non-hydrogen atoms was carried out to converge; $R = 6.3\%$. Scattering factors were taken from Cromer and Mann.[19] Anomalous dispersion terms were included for the rhodium, iron, and phosphorus atoms. Unit weights were used throughout. The largest peak in the final difference electron density map was 0.4 e Å^{-3}.

Results and Discussion

General Observations. As demonstrated by this and previous work,[9] the anionic ketenylidene cluster $[Fe_3(CO)_9(CCO)]^{2-}$ is a very useful starting material for the synthesis of heterometallic carbide clusters (Scheme I). The most successful cluster-building reactions occurred when the electrophilic transition-metal reagent is coordinatively unsaturated or contains labile ligands. It is interesting to note that the syntheses of $[PPN]_2[MFe_3(CO)_{13}C]$ (M = Cr, W) are readily reversed by dissolving the products in acetonitrile. For the synthesis of $[PPN][RhFe_3(CO)_{12}C]$ it is necessary to add a reagent to remove the free chloride from solution, and $[BzMe_3N][PF_6]$ was chosen. In several cases, the initially formed heterometallic carbide clusters are reactive toward further cluster building to produce penta- or hexanuclear clusters. Given this high degree of reactivity, it was often difficult to obtain pure compounds. The syntheses described in the Experimental Section reproducibly gave materials that were judged to be greater than 95% pure on the basis of their ^{13}C NMR spectra. These anionic clusters cannot be purified by chromatography, and in most cases repeated attempts to increase the purity via fractional crystallization failed. This is presumed to be due to the nearly identical solubilities of compounds with the same charge.

All of the clusters are moderately air- and moisture-sensitive, especially in solution. Infrared monitoring of solutions of $[MFe_3(CO)_{13}C]^{2-}$ (M = Cr, W) exposed to the atmosphere showed rapid decomposition to yield $[Fe_3(CO)_9(CCO)]^{2-}$, followed by slower decomposition (ca. 1 h) as indicated by the disappearance of all resonances in the CO stretching region. The iron–rhodium compounds appeared to be particularly sensitive in diethyl ether solutions, and therefore these clusters were handled in glassware that was treated with a silylating agent to remove surface hydroxyl groups.

The syntheses of all new compounds were found to be most conveniently monitored by IR spectroscopy. In general, the main band in the CO stretching region is an excellent indicator of the charge of a cluster. The value of this frequency increases by approximately 50 cm^{-1} with every incremental increase in charge (Table II). It was also useful to examine the region where the metal–carbide modes are observed, 950–550 cm^{-1}, as the presence of a band at approximately 900 cm^{-1} is a strong indicator that the system is a tetranuclear butterfly carbide species.[20] Unfortunately, the spectra for these compounds are quite complex and IR spectroscopy was not a good indicator of purity.

Table II. IR CO Stretching Frequencies for Heterometallic Carbide Clusters[a]

compd	medium	ν_{CO}, cm^{-1}
$[PPN]_2[CrFe_3(CO)_{13}C]$	CH_2Cl_2	2032 vw, 1972 sh, 1964 s, 1942 s, 1906 sh, 1880 sh, 1835 w, br, 1790 w, br
	Nujol	2028 w, 1960 s, 1930 s, 1917 sh, 1903 s, 1885 s, 1876 sh, 1840 m, 1787 m
$[PPN]_2[WFe_3(CO)_{13}C]$	CH_2Cl_2	2025 vw, 1973 sh, 1961 s, 1946 s, 1935 sh, 1904 m, sh, 1883 m, 1840 m
	Nujol	2030 vw, 1973 sh, 1959 s, 1944 s, 1927 s, 1915 sh, 1903 sh, 1885 m, 1879 sh, 1848 sh, 1843 m, 1815 m
$[PPN][RhFe_3(CO)_{12}C]$	CH_2Cl_2	2074 w, 2017 vs, 1979 s, 1962 m, 1944 w, sh
	Nujol	2075 w, 2018 sh, 2003 s, 1986 sh, 1977 s, 1957 s, 1949 s, 1939 s, 1922 s, 1910 sh
$[PPN]_2[Cr_2Fe_3(CO)_{16}C]$	CH_2Cl_2	2036 vw, 1977 s, 1960 s, 1947 s, sh, 1917 sh, 1880 w, br, 1780 w, br
	Nujol	2035 w, 1972 sh, 1947 s, 1933 sh, 1913 s, 1902 sh, 1877 s, 1870 sh, 1852 m, 1844 m, 1802 m, 1788 m
$Rh_2Fe_3(CO)_{14}C$	pentane	2106 vw, 2077 m, 2062 s, 2056 s, 2029 m, sh, 2021 m, 2012 m, sh, 1982 w, 1911 w
	Nujol	2107 w, 2079 s, sh, 2053 s, 2039 s, sh, 2024 sh, 2017 s, 2004 sh, 1988 s, 1960 s, 1937 s, 1903 sh, 1894 s, sh, 1888 s
$[PPN][Rh_3Fe_3(CO)_{15}C]$	CH_2Cl_2	2016 s, 1980 m, 1940 w, br, 1880 m, 1850 w, br
	Nujol	2024 sh, 2011 vs, 1992 m, 1976 s, 1946 m, 1926 m, 1907 m, 1883 m, 1848 s, 1832 m

[a] Legend: vs = very strong; s = strong; m = medium; w = weak; vw = very weak; sh = shoulder; br = broad.

Variable-temperature ^{13}C NMR spectroscopy was the most powerful tool for the assignment of solution structures. It was especially convenient in this work due to the availability of $[Fe_3(CO)_9(CCO)]^{2-}$ that is approximately 35% ^{13}C enriched at all of the carbon atoms. When this cluster was used as a starting material, the resulting carbide clusters were enriched at the carbide atom as well as the carbonyl carbons. Complete CO scrambling was observed in all cases, and this led to the enrichment of the carbonyls bound to the heterometals as well as the iron atoms. The carbide ligands are found to resonate far downfield from most other ligands and are therefore useful in identifying the products (Table III). For these systems, the carbide ligand also serves as an excellent internal standard for the integration of the intensity of the carbonyl ligands as long as care is taken in the data collection to allow for adequate nuclear relaxation.

Variable-Temperature ^{13}C NMR Study of $[PPN][RhFe_3(CO)_{12}C]$. The ^{13}C NMR spectrum of $[PPN][RhFe_3(CO)_{12}C]$ at −130 °C (Table III) is completely consistent with the solid-state structure.[9] In solution, this molecule contains a mirror plane that passes through the carbide ligand and the hinge metal atoms. The cluster has C_s symmetry, and eight resonances are predicted: one

(18) Stewart, J. M., Ed. "The XRAY System-Version of 1980"; Technical Report TR446; Computer Center, University of Maryland: College Park, MD, 1980.
(19) Cromer, D. T.; Mann, I. B.; *Acta Crystallogr., Sect. A: Cryst. Phys., Diffr., Theor. Gen. Crystallogr.* **1968**, *A24*, 321.
(20) Stanghellini, P. L.; Sailor, M. J.; Kuznesof, P.; Whitmire, K. H.; Hriljac, J. A.; Kolis, J. W.; Zheng, Y.; Shriver, D. F. *Inorg. Chem.*, following paper in this issue.
(21) Albano, V. G.; Chini, P.; Martinengo, S.; McCaffrey, D. J. A.; Strumolo, D.; Heaton, B. T. *J. Am. Chem. Soc.* **1974**, *96*, 8106.
(22) Heaton, B. T.; Strona, L.; Martinengo, S.; Strumolo, D.; Goodfellow, R. J.; Sadler, I. H. *J. Chem. Soc., Dalton Trans.* **1982**, 1499.
(23) Heaton, B. T.; Strona, L.; Martinengo, S.; Strumolo, D.; Albano, V. G.; Braga, D. *J. Chem. Soc., Dalton Trans.* **1983**, 2175.

Table III. ^{13}C NMR Data for Heterometallic Carbide Clusters[a,b]

compd	temp, °C	^{13}C NMR Data, ppm
$[PPN]_2[CrFe_3(CO)_{13}C]$[c,e]	−90	483.2 (1), 252.3 (1), 241.2 (2), 228.0 (1), 219.5 (6), 218.9 (2), 213.9 (1)
$[PPN]_2[CrFe_3(CO)_{13}C]$[d,e]	−120	482.5 (1), 254.3 (1), 242.0 (2), 228.2 (1), 221.2 (2), 220.7 (2), 219.7 (2), 219.1 (2), 214.9 (1)
$[PPN]_2[WFe_3(CO)_{13}C]$[c,e]	−90	470.1 (1) [J_{C-W} = 50 Hz], 220.2 (2), 218.6 (6), 212.0 (1)
$[PPN]_2[WFe_3(CO)_{13}C]$[d-f]	−120	470.0 (1), 238.3 (1), 222.4 (2), 221.0 (6), 217.3 (2), 213.4 (1), 205.3 (1)
$[PPN][MnFe_3(CO)_{13}C]$[c]	−80	468.4 (1), 237.5 (1), 224.1 (2), 215.0 (7), 214.0 (2), 208.7 (1)
$[PPN][MnFe_3(CO)_{13}C]$[d]	−120	467.8 (1), 238.1 (1), 224.5 (2), 216.4 (2), 215.1 (1), 215.0 (4), 214.4 (2), 209.2 (1)
$[PPN][RhFe_3(CO)_{12}C]$[c]	−50	461.3 (1) [d J_{C-Rh} = 18 Hz], 218.1 (3), 215.9 (6), 190.4 (3), [d, J_{C-Rh} = 66 Hz]
$[PPN][RhFe_3(CO)_{12}C]$[d,f]	−130	460.1 (1), 222.0 (2), 218.9 (2), 215.6 (2), 213.8 (2), 211.4 (1), 194.3 (2), 181.6 (1)
$[PPN]_2[Cr_2Fe_3(CO)_{16}C]$[c]	−90	496.2 (1), 252.0 (2), 237.8 (4), 223.9 (2), 221.1 (6), 217.5 (2)
$Rh_2Fe_3(CO)_{14}C$[c]	−90	457.3 (1) [t, J_{C-Rh} = 27 Hz], 221.5 (1) [t, J_{C-Rh} = 39 Hz], 214.2 (2), 210.5 (3), 210.3 (2), 204.5 (2), 186.0 (2) [d, J_{C-Rh} = 72 Hz], 177.0 (2) [d, J_{C-Rh} = 70 Hz]
$[PPN][Rh_3Fe_3(CO)_{15}C]$[c]	−90	450.8 (1) [q, J_{C-Rh} = 19 Hz], 230.4 (3) [t, J_{C-Rh} = 39 Hz], 214.4 (9), 194.9 (3) [d, J_{C-Rh} = 93 Hz]

[a] All shifts are reported downfield of TMS with the solvent resonance (CD_2Cl_2, δ = 53.8) as an internal reference. [b] The numbers in parentheses are the relative intensities. [c] Spectra recorded in CD_2Cl_2/CH_2Cl_2 (ca. 1:3). [d] Spectra recorded in $CD_2Cl_2/CHFCl_2$ (ca. 1:3). [e] Sample dissolved at −78 °C and inserted into a precooled NMR probe. [f] Due to extreme line broadening, coupling data could not be obtained.

for the carbide ligand, two due to the carbonyls bound to the rhodium atom, two from the carbonyls bound to the unique iron atom, and three associated with the carbonyls bound to the symmetry-related wing-tip iron atoms. Furthermore, all peaks assigned to ligands bound to the rhodium atom should be doublets due to spin–spin coupling (^{103}Rh, 100% abundance, $I = {}^1/_2$).

The variable-temperature spectra from −130 to −40 °C for $[PPN][RhFe_3(CO)_{12}C]$ contain one resonance far downfield of the others, which is readily assigned to the carbide ligand.[2] At low temperatures all of the resonances are broadened due to high solvent viscosity and temperature gradients within the solution, but at higher temperatures the downfield resonance is clearly a doublet with $^1J_{C-Rh}$ equal to 18 Hz. This value is slightly higher than that observed in trigonal-prismatic rhodium clusters (Table IV).

The remaining seven resonances are in the region typical for terminal carbonyl ligands, approximately 170–235 ppm. An examination of the variable-temperature behavior clearly separates these into three sets. The first set consists of the two upfield peaks which are integrated in the ratio 2:1. When the system is warmed, these resonances broaden, collapse, and then coalesce to a doublet at 191 ppm, and they are assigned to the carbonyl ligands bonded to the rhodium atom ($^1J_{C-Rh}$ = 66 Hz). The second set is composed of the peaks at 220.2 and 211.4 ppm, which collapse to a single resonance (219 ppm) upon warming. These are assigned

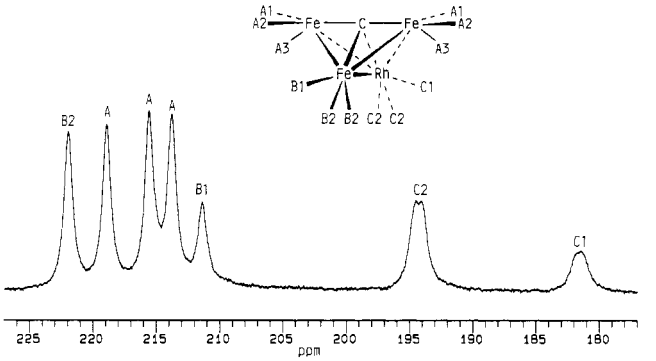

Figure 1. Carbonyl region of the ^{13}C NMR spectrum (100.577 MHz) of $[PPN][RhFe_3(CO)_{12}C]$ in $CD_2Cl_2/CHFCl_2$ (1:3) at −130 °C and the proposed peak assignments.

Table IV. Values of $^1J_{C(carbide)-Rh}$ for Carbide Clusters

compd	$^1J_{C-Rh}$, Hz	ref
$[RhFe_3(CO)_{12}C]^-$	18	*a*
$Rh_2Fe_3(CO)_{14}C$	27	*a*
$[Rh_3Fe_3(CO)_{15}C]^-$	19	*a*
$[Rh_6(CO)_{15}C]^{2-}$	14	21
$[HRh_6(CO)_{15}C]^-$	10, 15	22
$[Rh_6(CO)_{15}C(AuPEt_3)]^-$	11, 13	23

[a] This work.

to the ligands bonded to the hinge iron atom. The third set consists of three peaks of intensity 2, which are located at 218.9, 215.6, and 213.8 ppm. When the system is warmed, these also simultaneously broaden, collapse, and then form a single peak. These resonances are due to the carbonyl ligands on the symmetry-related wing-tip metals. The low-temperature limiting spectrum and the peak assignments are shown in Figure 1.

The spectrum at −40 °C consists of three carbonyl resonances that are integrated in the ratio 3:6:3 vs. the carbide ligand. The only fluxional process that is occurring is fast metal-localized carbonyl exchange. This is a common low-energy fluxional process in cluster compounds[24] and is the lowest energy process observed for other butterfly carbide clusters.[25] Further warming of the sample causes a simultaneous broadening and collapse of all three of these peaks. The room-temperature spectrum consists of a single broad signal at 216 ppm, which indicates that the carbonyl ligands are now completely mobile over the entire metal framework.

Variable-Temperature ^{13}C NMR Studies of $[PPN]_2[MFe_3(CO)_{13}C]$ (M = Cr, W). Both of these clusters contain one more carbonyl ligand than $[PPN][RhFe_3(CO)_{12}C]$. On the basis of the 18-electron rule, it is expected that the extra ligand will be associated with the heterometal. The IR spectra of these clusters (Table II) contain low-frequency vibrations at approximately 1800 cm^{-1}, which indicates the presence of bridging carbonyls.

Initial attempts to assign the resonances in the low-temperature spectra of $[PPN]_2[MFe_3(CO)_{13}C]$ (M = Cr, W) were unsuccessful. A closer examination of the low-temperature spectra of the tungsten compound revealed a small peak at 463.8 ppm, which is attributed to a second carbide species. This integrates as approximately 1:8 vs. the major carbide peak. When the solid sample was dissolved at −78 °C and the NMR tube quickly placed into a precooled spectrometer, the second species was not observed. A series of experiments demonstrated that the second species does not appear until the sample is warmed above 0 °C. Subsequent studies of the chromium cluster demonstrated a similar phenomenon. In this case a second resonance assignable to a carbide ligand was not observed. As discussed below, the major species are butterfly carbide clusters with the heterometals occupying hinge positions. The other species may be isomers with the heterometals on a wing tip.

(24) Band, E.; Muetterties, E. L. *Chem. Rev.* **1978**, *78*, 639.
(25) Davis, J. H.; Beno, M. A.; Williams, J. M.; Zimmie, J.; Tachikawa, M.; Muetterties, E. L. *Proc. Natl. Acad. Sci. U.S.A.* **1981**, *78*, 668.

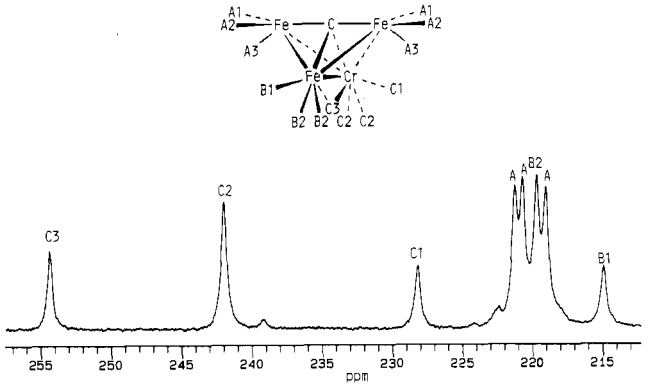

Figure 2. Carbonyl region of the ^{13}C NMR spectrum (100.577 MHz) of $[PPN]_2[CrFe_3(CO)_{13}C]$ in $CD_2Cl_2/CHFCl_2$ (1:3) at −120 °C and the proposed peak assignments.

The spectrum at −120 °C of $[PPN]_2[CrFe_3(CO)_{13}C]$, which had been dissolved at −78 °C, consists of nine resonances which are integrated in the ratio 1:1:2:1:2:2:2:2:1. The downfield resonance at 482.5 ppm is due to the carbide carbon. The eight carbonyl peaks form three sets. The first of these is composed of the three peaks at 254.3, 242.0, and 228.2 ppm (intensities 1:2:1). When the system is warmed, these coalesce into a single resonance at 242 ppm. The second set of signals at 221.2, 220.7, and 219.1 ppm (intensities 2:2:2) coalesce upon warming into a peak of intensity 6. The final set consists of the two peaks at 219.7 and 214.9 ppm, which are integrated in the ratio 2:1. These sets are assigned to the carbonyl ligands on the chromium atom, two related iron atoms, and a unique iron atom, respectively. The downfield resonance at 254 ppm is attributed to a bridging carbonyl. As was discussed for $[PPN][RhFe_3(CO)_{12}C]$, $[Fe_4(CO)_{12}C]^{2-}$,[25] and $[HFe_4(CO)_{12}C]^-$,[25] the lowest energy fluxional process for butterfly carbide clusters is fast carbonyl exchange localized on single metal centers. At low temperatures where this localized exchange process has been stopped for the carbonyl groups attached to the chromium and a unique iron atom, a symmetry element appears to be present that relates the CO ligands bonded to the two remaining iron atoms. If the chromium atom were to occupy a wing-tip site, the bridging carbonyl would probably span a wing-tip–hinge bond and the cluster would be asymmetric, in disagreement with the NMR data. The NMR data are satisfied by placement of the chromium atom in a hinge position, which should lead to a bridging carbonyl group across the hinge bond and thus establish a mirror plane. Therefore, the structure appears to be analogous to that of $Fe_4(CO)_{13}C$ with the chromium atom occupying a hinge position.[26] The low-temperature limiting spectrum and peak assignments are shown in Figure 2.

The spectra of $[PPN]_2[WFe_3(CO)_{13}C]$, which has been dissolved at low temperature, are very similar to those of $[PPN][CrFe_3(CO)_{13}C]$. The carbide resonance of this cluster displays satellites due to coupling with the tungsten atom (^{183}W, 14.28% abundance, $I = {}^1/_2$). It is also important to note that the resonance due to the coalescence of peaks at 238.3, 222.4, and 205.3 ppm (ratio 1:2:1) also displays satellites with $^1J_{C-W} = 133$ Hz, confirming that these resonances arise from the carbonyl ligands bonded to the tungsten atom. This set is analogous to the first set discussed for the chromium analogue. Unfortunately, there appears to be overlap of three resonances of intensity 2 in the low-temperature spectrum. However, the same structural assignment may be made for this cluster as was discussed for the chromium analogue. The low-temperature limiting spectrum and peak assignment are shown in Figure 3.

Variable-Temperature ^{13}C NMR Study of $[PPN][MnFe_3(CO)_{13}C]$. The variable-temperature ^{13}C NMR spectra of $[PPN][MnFe_3(CO)_{13}C]$[9] have also been recorded to −120 °C (Table III). These appear analogous to that observed for $[PPN]_2[MFe_3(CO)_{13}C]$ (M = Cr, W). Once again the most important feature is a peak with an intensity of 6 that is observed after metal-localized carbonyl exchange has stopped for the carbonyls bonded to the manganese and unique iron atoms. This cluster is also proposed to contain a butterfly metal core with the bridging carbonyl across the hinge bond.

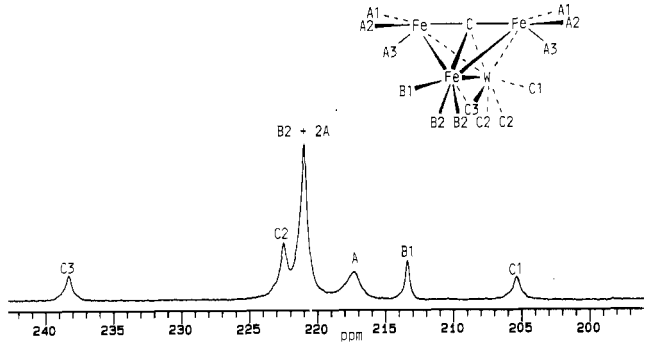

Figure 3. Carbonyl region of the ^{13}C NMR spectrum (100.577 MHz) of $[PPN]_2[WFe_3(CO)_{13}C]$ in $CD_2Cl_2/CHFCl_2$ (1:3) at −120 °C and the proposed peak assignments.

Thermolysis of $[PPN]_2[MFe_3(CO)_{13}C]$ (M = Cr, W). Acetone solutions of these clusters were heated in sealed NMR tubes to approximately 55 °C. The ^{13}C NMR spectrum of the chromium cluster revealed a slow disproportionation to yield $[Cr_2Fe_3(CO)_{16}C]^{2-}$ and $[Fe_3(CO)_9(CCO)]^{2-}$ (eq 1). The reaction was

$$2[CrFe_3(CO)_{13}C]^{2-} \xrightarrow{\Delta} [Fe_3(CO)_9(CCO)]^{2-} + [Cr_2Fe_3(CO)_{16}C]^{2-} \quad (1)$$

approximately 75% complete after 32 h. For the tungsten compound a new resonance was observed at 459 ppm. This does not correspond to a known compound and is assigned to $[W_2Fe_3(CO)_{16}C]^{2-}$. This disproportionation is much slower and is only approximately 5% complete after 32 h.

Attempted Synthesis of $[PPN]_2[MoFe_3(CO)_{13}C]$. Attempts were made to synthesize this cluster in a reaction analogous to that for the chromium and tungsten analogues. Infrared spectroscopy indicated that when stoichiometric quantities of $[PPN]_2[Fe_3(CO)_9(CCO)]$ and $Mo(CO)_3(NCMe)_3$ are allowed to react in acetone solution a new product is formed but a significant quantity of the triiron cluster remains. When 2 equiv of the molybdenum reagent is used, the reaction goes to completion. The new cluster that is produced contains a main band in the CO stretching region at ca. 1955 cm^{-1}. Upon continued stirring, this cluster disappears and a new product with a main band at 1970 cm^{-1} is formed. Subsequent ^{13}C NMR studies confirmed these observations and also show that the initial carbide resonance at 475.8 ppm (acetone-d_6, −90 °C) is replaced by a second resonance at 472.5 ppm over the course of approximately 3 h. This facile interconversion frustrated attempts to isolate the initially formed products.

$[PPN]_2[Cr_2Fe_3(CO)_{16}C]$. When $[PPN]_2[Fe_3(CO)_9(CCO)]$ is allowed to react with an excess of $Cr(CO)_3(NCMe)_3$, a new compound is formed. Spectroscopic data fit the formation $[PPN]_2[Cr_2Fe_3(CO)_{16}C]$ (Tables II and III). No further reaction to yield a higher nuclearity cluster was observed at room temperature. The ^{13}C NMR spectrum at room temperature consists of two peaks at 499.8 and 229.8 ppm. Upon cooling, the carbonyl resonance collapses and is replaced by five resonances that are integrated in the ratio 2:4:2:6:2. Electron-counting considerations predict a square-pyramidal metal core. The positions of the iron and chromium atoms could not be unambiguously assigned.

$Rh_2Fe_3(CO)_{14}C$. Initial attempts to synthesize $[RhFe_3(CO)_{12}C]^-$ via eq 2 by using an excess of $[Rh(CO)_2Cl]_2$ led to the isolation of two higher nuclearity clusters. The first of these is

$$[Fe_3(CO)_9(CCO)]^{2-} + [Rh(CO)_2Cl]_2 \rightarrow [RhFe_3(CO)_{12}C]^- + [Rh(CO)_2Cl_2]^- \quad (2)$$

formulated as $Rh_2Fe_3(CO)_{14}C$ (Tables II and III). A better route

(26) Bradley, J. S.; Ansell, G. B.; Leonowicz, M. E.; Hill, E. W. *J. Am. Chem. Soc.* **1981**, *103*, 4968.

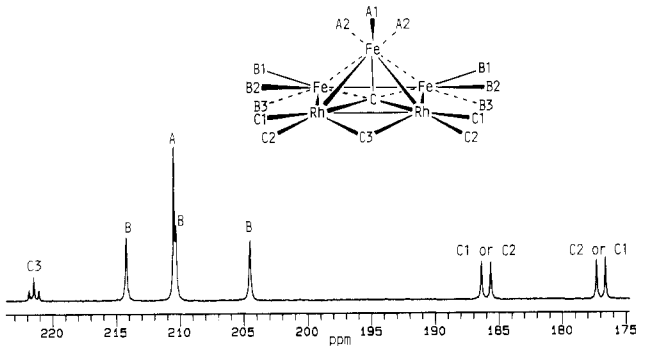

Figure 4. Carbonyl region of the ^{13}C NMR spectrum (100.577 MHz) of $Rh_2Fe_3(CO)_{14}C$ in CD_2Cl_2 at −90 °C and the proposed peak assignments.

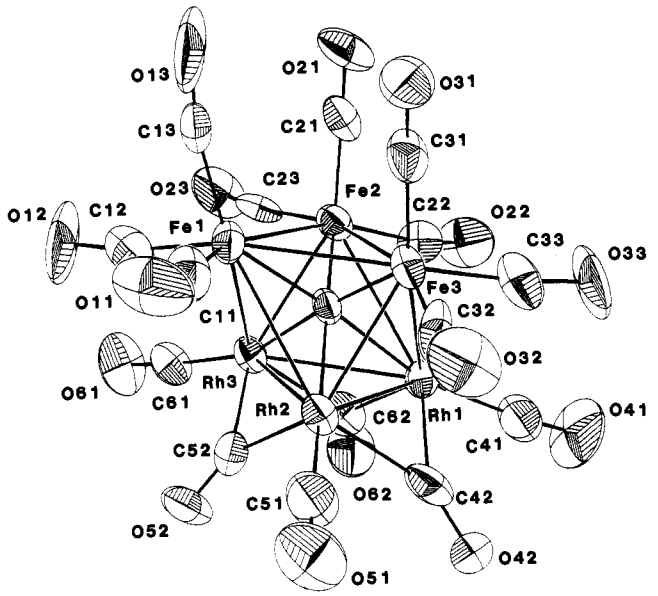

Figure 5. ORTEP diagram of the cluster anion in $[PPN][Rh_3Fe_3(CO)_{15}C]$ showing the atomic labeling scheme.

to this compound was achieved by employing $[RhFe_3(CO)_{12}C]^-$ in a redox-condensation reaction (eq 3). This reaction works best

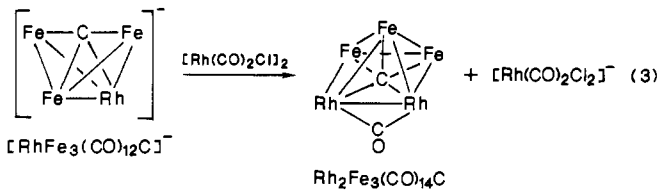

in diethyl ether or toluene solutions, as $[PPN][Rh(CO)_2Cl_2]$ precipitates. In more polar solvents (CH_2Cl_2, THF) this anion is soluble and leads to a hexanuclear cluster. This will be described later. During the course of this work the same cluster was also isolated via a different reaction.[27]

The variable-temperature ^{13}C NMR spectra of $Rh_2Fe_3(CO)_{14}C$ contain the carbide resonance at 457 ppm as a triplet due to coupling to two equivalent rhodium nuclei (J = 27 Hz) Table IV). There is also a resonance at 222 ppm that shows coupling to both rhodium atoms and is attributed to a bridging carbonyl group. The two upfield carbonyl resonances are doublets with $^1J_{C-Rh}$ equal to 72 and 70 Hz, respectively. These are assigned to terminal carbonyls bonded to the rhodium atoms and are integrated at intensity 2 vs. the carbide ligand. The low-temperature spectrum contains three peaks at 214.2, 210.3, and 204.5 ppm. When the solution is warmed, these coalesce into a resonance at 210 ppm with an integrated intensity of 6. Another peak with an intensity of 3 occurs throughout the temperature range studied and is located at 210.5 ppm. This 74-CVE cluster appears to be a square pyramid of metals with the carbide ligand located in the center of the square face. The only structure consistent with the NMR data is shown in Figure 4, along with the proposed peak assignments.

$[PPN][Rh_3Fe_3(CO)_{15}C]$. As mentioned previously, the reaction of $[Fe_3(CO)_9(CCO)]^{2-}$ with an excess of $[Rh(CO)_2Cl]_2$ gives a complex mixture of products. A third cluster that has been isolated from this system is the hexanuclear anion $[Rh_3Fe_3(CO)_{15}C]^-$

Table V. Selected Bond Distances (Å) and Angles (deg) with Estimated Standard Deviations for $[PPN][Rh_3Fe_3(CO)_{15}C]$[a]

Fe1–Fe2	2.687 (4)	Fe3–C33	1.79 (2)
Fe1–Fe3	2.695 (4)	Rh1–C41	1.92 (2)
Fe2–Fe3	2.696 (4)	Rh1–C42	2.05 (2)
Rh1–Rh2	2.762 (2)	Rh1–C62	2.11 (2)
Rh1–Rh3	2.775 (2)	Rh2–C51	1.90 (2)
Rh2–Rh3	2.770 (2)	Rh2–C52	2.05 (2)
Fe1–Rh3	2.774 (3)	Rh2–C42	2.07 (2)
Fe1–Rh2	2.815 (4)	Rh3–C61	1.89 (2)
Fe2–Rh1	2.789 (4)	Rh3–C62	2.08 (2)
Fe2–Rh3	2.818 (4)	Rh3–C52	2.06 (2)
Fe3–Rh1	2.804 (3)	C11–O11	1.14 (3)
Fe3–Rh2	2.787 (3)	C12–O12	1.16 (3)
Fe1–C99	1.88 (2)	C13–O13	1.18 (3)
Fe2–C99	1.86 (2)	C21–O21	1.15 (2)
Fe3–C99	1.87 (2)	C22–O22	1.14 (3)
Rh1–C99	2.03 (2)	C23–O23	1.15 (2)
Rh2–C99	2.05 (2)	C31–O31	1.14 (2)
Rh3–C99	2.04 (2)	C32–O32	1.14 (3)
Fe1–C11	1.79 (2)	C33–O33	1.14 (2)
Fe1–C12	1.79 (2)	C41–O41	1.08 (3)
Fe1–C13	1.77 (2)	C42–O42	1.15 (2)
Fe2–C21	1.78 (2)	C51–O51	1.13 (3)
Fe2–C22	1.82 (2)	C52–O52	1.17 (2)
Fe2–C23	1.80 (2)	C61–O61	1.14 (2)
Fe3–C31	1.78 (2)	C62–O62	1.13 (3)
Fe3–C32	1.84 (2)		
Fe2–Fe1–Fe3	60.11 (10)	Fe1–Rh3–Fe2	57.43 (9)
Fe2–Fe1–Rh3	62.10 (9)	Fe1–C99–Rh1	174.8 (10)
Fe2–Fe1–Rh2	90.71 (9)	Fe2–C99–Rh2	175.7 (10)
Fe3–Fe1–Rh3	91.34 (10)	Fe3–C99–Rh3	175.1 (10)
Fe3–Fe1–Rh2	60.72 (8)	Fe1–C99–Fe2	91.8 (7)
Rh3–Fe1–Rh2	59.42 (8)	Fe1–C99–Fe3	92.0 (8)
Fe1–Fe2–Fe3	60.10 (10)	Fe2–C99–Fe3	92.4 (7)
Fe1–Fe2–Rh1	90.80 (10)	Rh1–C99–Rh2	85.2 (6)
Fe1–Fe2–Rh3	60.48 (9)	Rh1–C99–Rh3	85.9 (7)
Fe3–Fe2–Rh1	61.47 (8)	Rh2–C99–Rh3	85.0 (6)
Fe3–Fe2–Rh3	90.39 (10)	Fe1–C99–Rh2	91.4 (7)
Rh1–Fe2–Rh3	59.34 (8)	Fe1–C99–Rh3	90.0 (6)
Fe1–Fe3–Fe2	59.79 (10)	Fe2–C99–Rh1	91.4 (7)
Fe1–Fe3–Rh1	90.30 (10)	Fe2–C99–Rh3	92.1 (8)
Fe1–Fe3–Rh2	61.76 (9)	Fe3–C99–Rh1	91.9 (6)
Fe2–Fe3–Rh1	60.90 (9)	Fe3–C99–Rh2	90.4 (7)
Fe2–Fe3–Rh2	91.13 (10)	Fe1–C11–O11	171.9 (18)
Rh1–Fe3–Rh2	59.19 (8)	Fe1–C12–O12	167.9 (21)
Rh2–Rh1–Rh3	60.05 (5)	Fe1–C13–O13	178.4 (17)
Rh2–Fe1–Fe3	60.10 (7)	Fe2–C21–O21	179.1 (20)
Rh2–Fe1–Fe2	89.73 (7)	Fe2–C22–O22	169.1 (18)
Rh3–Rh1–Fe3	89.06 (7)	Fe2–C23–O23	171.6 (18)
Rh3–Rh1–Fe2	60.85 (7)	Fe3–C31–O31	176.6 (19)
Fe3–Rh1–Fe2	57.62 (9)	Fe3–C32–O32	167.3 (19)
Rh1–Rh2–Rh3	60.22 (6)	Fe3–C33–O33	172.8 (21)
Rh1–Rh2–Fe1	88.74 (7)	Rh1–C41–O41	172.7 (23)
Rh1–Rh2–Fe3	60.72 (7)	Rh1–C42–O42	138.8 (16)
Rh3–Rh2–Fe1	59.56 (7)	Rh1–C62–O62	136.3 (16)
Rh3–Rh2–Fe3	89.51 (8)	Rh2–C51–O51	177.6 (19)
Fe1–Rh2–Fe3	57.51 (9)	Rh2–C52–O52	138.2 (16)
Rh1–Rh3–Rh2	59.73 (5)	Rh2–C42–O42	137.5 (17)
Rh1–Rh3–Fe1	89.29 (7)	Rh3–C61–O61	173.5 (17)
Rh1–Rh3–Fe2	59.81 (7)	Rh3–C62–O62	140.4 (17)
Rh2–Rh3–Fe1	61.02 (8)	Rh3–C52–O52	136.8 (15)
Rh2–Rh3–Fe2	88.95 (8)		

[a] Derived results for the PPN cation are in the supplementary material.

(27) Lopatin, V. E.; Ershova, V. A.; Tsybenov, M. Ts.; Gubin, S. P. *Izv. Akad. Nauk SSSR, Ser. Khim.* **1984**, 2648.

Table VI. Positional Parameters with Estimated Standard Deviations for the Anion of $[PPN][Rh_3Fe_3(CO)_{15}C]$[a]

atom	x (σ(X))	y (σ(y))	z (σ(z))
Fe1	0.6902 (1)	−0.0058 (3)	0.6643 (1)
Fe2	0.8145 (2)	0.1836 (3)	0.6681 (1)
Fe3	0.8483 (1)	−0.0953 (3)	0.6522 (1)
Rh1	0.8778 (1)	0.1111 (2)	0.5944 (0)
Rh2	0.7520 (1)	−0.0874 (2)	0.5902 (0)
Rh3	0.7140 (1)	0.1980 (2)	0.6067 (0)
O11	0.6040 (12)	−0.2769 (20)	0.6534 (5)
O12	0.5362 (10)	0.1601 (26)	0.6645 (6)
O13	0.6748 (9)	−0.0266 (18)	0.7482 (4)
O21	0.8423 (10)	0.1534 (17)	0.7490 (4)
O22	0.9726 (10)	0.3368 (21)	0.6529 (5)
O23	0.7173 (11)	0.4495 (18)	0.6817 (5)
O31	0.8510 (9)	−0.2006 (18)	0.7301 (4)
O32	0.8479 (11)	−0.3905 (16)	0.6221 (5)
O33	1.0283 (8)	−0.0678 (26)	0.6414 (5)
O41	1.0484 (10)	0.1846 (27)	0.5604 (6)
O42	0.8834 (8)	−0.0754 (17)	0.5243 (4)
O51	0.7056 (10)	−0.3581 (17)	0.5485 (5)
O52	0.6241 (8)	0.0558 (15)	0.5449 (4)
O61	0.5860 (10)	0.4278 (18)	0.5964 (5)
O62	0.8249 (10)	0.3668 (19)	0.5487 (5)
C99	0.7836 (9)	0.0493 (20)	0.6325 (5)
C11	0.6406 (12)	−0.1732 (24)	0.6552 (6)
C12	0.5996 (14)	0.1023 (27)	0.6608 (6)
C13	0.6817 (10)	−0.0168 (23)	0.7147 (6)
C21	0.8316 (11)	0.1642 (21)	0.7171 (6)
C22	0.9130 (13)	0.2716 (21)	0.6554 (6)
C23	0.7515 (12	0.3431 (21)	0.6743 (5)
C31	0.8505 (12)	−0.1556 (22)	0.7001 (6)
C32	0.8422 (11)	−0.2748 (24)	0.6305 (6)
C33	0.9579 (12)	−0.0745 (25)	0.6434 (7)
C41	0.9848 (13)	0.1625 (27)	0.5707 (7)
C42	0.8540 (12)	−0.0368 (23)	0.5534 (6)
C51	0.7212 (13)	−0.2561 (25)	0.5642 (7)
C52	0.6732 (11)	0.0557 (21)	0.5675 (5)
C61	0.6370 (12)	0.3447 (21)	0.5985 (6)
C62	0.8119 (13)	0.2823 (23)	0.5716 (6)

[a] Positional parameters for the PPN cation are in the supplementary material.

(Tables II and III). The formation of this cluster proceeds slowly in dichloromethane (ca. 12 h) and is much more rapid in THF (ca. 2 h). The reaction pathway is believed to follow eq 4 because

$$[Fe_3(CO)_9(CCO)]^{2-} + 2[Rh(CO)_2Cl]_2 \rightarrow Rh_2Fe_3(CO)_{14}C + 2[Rh(CO)_2Cl_2]^- \rightarrow [Rh_3Fe_3(CO)_{15}C]^- \quad (4)$$

$Rh_2Fe_3(CO)_{14}C$ was detected in the IR spectrum during the early stages of the reaction. Other products are believed to be formed during this reaction but have not been reproducibly isolated. During the course of this work this cluster was also isolated by other workers.[28]

The X-ray crystal structure of $[PPN][Rh_3Fe_3(CO)_{15}C]$ was determined. An ORTEP diagram is shown in Figure 5. Selected bond angles and distances are listed in Table V and positional parameters in Table VI. This is the first structurally characterized $M_3M'_3$ carbide cluster.

The cluster anion exists as a trigonal-antiprismatic metal skeleton enclosing the carbide atom. Three iron atoms form one face of the polyhedron, and the rhodium atoms define the other. This maximizes the number of homometallic bonds. The iron atoms each bear three carbonyl ligands, two of which are terminal and one of which is weakly semibridging (average Fe–C–O = 168 (1)°). The rhodium atoms define a triangle with one terminal carbonyl ligand per rhodium atom and one carbonyl group symmetrically bridging each edge. The carbide atoms is within the metal framework and is located slightly closer to the iron face (Fe–C99 = 1.87 (1) Å; Rh–C99 = 2.04 (1) Å). The coordination of the carbide ligand is nearly octahedral (Fe–C99–Fe = 92.1 (3)°; Rh–C99–Rh = 85.4 (5)°; Fe–C–Rh = 91.2 (8) or 175.3 (6)°).

The ^{13}C NMR spectra are consistent with the solid-state structure. At room temperature peaks are observed at 452.2 and 213.9 ppm. The carbide resonance is a quartet with $^1J_{C-Rh}$ = 19 Hz. When the system is cooled, the carbonyl resonance is replaced by three resonances at 230.4 (t, $^1J_{C-Rh}$ = 39 Hz), 214.4, and 194.9 (d, J_{C-Rh} = 93 Hz) ppm. These are assigned to the bridging carbonyls, the carbonyls on the iron face, and the terminal groups on the rhodium atoms, respectively.

Conclusions

The anionic ketenylidene cluster $[Fe_3(CO)_9(CCO)]^{2-}$ is an excellent precursor to a wide variety of tetra-, penta-, and hexanuclear heterometallic carbide clusters. In most cases a sequence of selective additions of the heterometal fragments is observed. The tetranuclear systems are butterfly clusters, and there is a strong preference for the heterometal to occupy a hinge position. For the Fe/Rh clusters additional cluster-building products contain the metals in segregated groups, which maximize the number of homometallic metal–metal bonds.

Acknowledgment. This research was supported by the Department of Energy through Grants DE-AC02-83ER13104 and DE-FG02-86ER13640.

Supplementary Material Available: Listings of bond distances and angles, positional parameters, and anisotropic thermal parameters for $[PPN][Rh_3Fe_3(CO)_{15}C]$ (5 pages); listings of F_{obsd} and F_{calcd} for $[PPN][Rh_3Fe_3(CO)_{12}C]$ (54 pages). Ordering information is given on any current masthead page.

(28) Gubin, S. P.; Mikova, N. M.; Tsybenov, M. Ts.; Lopatin, V. E. *Koord. Khim.* **1984**, *10*, 625.